Homochiral and Heterochiral Dimers of the Methylzinc Alkoxide Formed from Dimethylzinc and Enantiomeric 3-*exo*-(Dimethylamino)isoborneol—Origin of the Distinct Differences in Solution-Phase Behavior and Crystal Structures

Masato Kitamura, Masashi Yamakawa, Hiromasa Oka, Seiji Suga, and Ryoji Noyori*

Abstract: Dimethylzinc reacts with (2*S*)- or (2*R*)-3-*exo*-(dimethylamino)isoborneol [(2*S*)- or (2*R*)-DAIB] to eliminate methane and produce a tricoordinate methylzinc aminoalkoxide, which forms a dimeric structure. The homochiral dimerization of the enantiomeric compound leads to the chiral, (*S*,*S*) or (*R*,*R*) dinuclear Zn complex, while the heterochiral interaction forms the *meso* (*S*,*R*) dinuclear compound. In both solution and crystalline state, the heterochiral dimer is more stable than the homochiral dimer. This stability difference in solution is the origin of the chirality amplification observed in the amino alcohol promoted asymmetric addition of dimethylzinc to benzaldehyde. In toluene, the homochiral dimer dissociates more readily into the monomer than the heterochiral isomer and also undergoes dissociation of the N–Zn dative bond making the two *N*-methyl groups equivalent. The differences in solution behavior between the diastereomers can be understood by comparing their crystal structures. X-ray analysis indicates that the labile Zn–O and Zn–N bonds in the (*S*,*S*) dimer are longer than those in the (*S*,*R*) isomer. Skeletal congestion caused by the polycyclic framework is the prime factor determining the properties of the dinuclear Zn complexes, with both steric and electronic factors governing their geometries. The distances between the C-2 proton and N–CH_3 of the other DAIB moiety in the homochiral dimer are close to the sum of the van der Waals radii. A significant nuclear Overhauser effect is seen between these protons in the homochiral dimer. The tetrahedral Zn atoms in the dinuclear complexes are linked covalently to the methyl group, to two oxygen atoms through covalent/electrostatic hybrid bonds, and to the dimethylamino group through electrostatic interaction. The repulsive interaction of the 1,3-*syn*-oriented Zn–CH_3 bonds significantly contributes to the lower stability of the homochiral dimeric complex. The N–Zn interaction in the homochiral dimer is labile, owing to the increase in the electrostatic interaction between the Zn atom and the neighboring oxygen atoms. This view is supported by the ab initio molecular orbital calculations of the model systems.

Keywords
ab initio calculations · asymmetric alkylations · catalysis · structure elucidation · zinc complexes

Introduction

With the growing significance of asymmetric catalysis,[1] synthetic chemists have started to examine precise coordination chemistry of main group metal compounds with neutral or anionic heteroatom ligands. Properties such as coordination number of metals, geometry, stability, and reactivity are subtly influenced by electronic and steric factors.[2–5] Slight structural changes sometimes have remarkable chemical consequences. Organozinc complexes formed from chiral β-dialkylamino alcohols and dialkylzincs present a typical example. As shown in Scheme 1, asymmetric addition of dialkylzincs to prochiral aldehydes is accomplished in the presence of a small amount of (2*S*)-3-*exo*-(dimethylamino)isoborneol [(2*S*)-DAIB] in hydrocarbon solvents.[6, 7] The enantiomerically pure catalyst in the methylation reaction displays an excellent level of enantioselectivity ((*S*):(*R*) = 96:4). Furthermore, the reaction shows a marked nonlinear relationship between the enantiomeric purity of the DAIB auxiliary and the alcoholic product; catalysis with DAIB in 20% *ee* produces the (*S*) alcohol in up to 88% *ee*

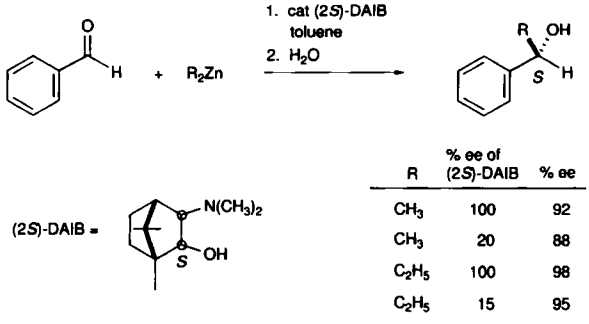

R	% ee of (2*S*)-DAIB	% ee
CH_3	100	92
CH_3	20	88
C_2H_5	100	98
C_2H_5	15	95

Scheme 1. Asymmetric alkylation of benzaldehyde with dialkylzincs promoted by (2*S*)-DAIB.

[*] Prof. R. Noyori, M. Kitamura, H. Oka, S. Suga
Department of Chemistry and Molecular Chirality Research Unit
Nagoya University, Chikusa, Nagoya 464-01 (Japan)
Fax: Int. code +(52)783-4177
M. Yamakawa
Kinjo Gakuin University, Omori, Moriyama, Nagoya 463 (Japan)

  0947-6539/96/0209-1173 $ 15.00+.25/0

((*S*):(*R*) = 94:6).[6b, c, 7a, 8, 9] The ethylation reaction using diethylzinc exhibited an even higher degree of enantioselectivity and chirality amplification (Scheme 1).[10] This unusual phenomenon is explained by the behavior of the chiral organozinc compound illustrated in Scheme 2. Dimethylzinc reacts with (2*S*)- or (2*R*)-DAIB to form the tricoordinate Zn compound (*S*)- or (*R*)-**2**, which serves as a catalyst promoting the asymmetric addition of dimethylzinc to benzaldehyde. The coordinatively unsaturated catalysts **2**, however, are in equilibrium with the dimers **1**. Because of the unique three-dimensional structure of the DAIB auxiliary, the dimerization occurs stereoselectively. Homochiral dimerization of (*S*)-**2** gives, out of three possible isomers, only (*S*,*S*)-**1**, which is characterized by the (*S*,*S*) configuration at the tetrahedral Zn atoms as well as the *syn* geometry of the central 5/4/5-fused tricyclic framework. Similarly, the heterochiral interaction of (*S*)-**2** and (*R*)-**2** leads, among four possibilities, solely to (*S*,*R*)-**1** possessing the (*S*,*R*) configuration at the Zn atoms and the *anti*-5/4/5 ring system. When both enantiomers (*S*)- and (*R*)-**2** coexist, the heterochiral combination occurs preferentially, since (*S*,*R*)-**1** is by far more stable than (*S*,*S*)- or (*R*,*R*)-**1** in a hydrocarbon solution. For example, the molecular weight measurement by vapor-pressure osmometry indicates that the dissociation constant of (*S*,*S*)-**1** is 3000 times larger than that of (*S*,*R*)-**1** in toluene at 40 °C ($K_{homo} \approx 3 \times 10^{-2}$ vs. $K_{hetero} \approx 1 \times 10^{-5}$).[11] The higher stability of the heterochiral dimer ($\Delta G \approx 29$ kJ mol^{-1}) relative to the homochiral dimers ($\Delta G = 9$ kJ mol^{-1}) results in the marked chirality amplification in the asymmetric alkylation.[6] However, the actual origin of the stability difference between the stereoisomers has remained unclear. We disclose here the structural characteristics of the diastereomeric complexes **1** in solution and in the crystalline state. This correlation, coupled with the ab initio calculations of model systems, leads to a deeper understanding of the organozinc chemistry.[6, 7, 12, 13]

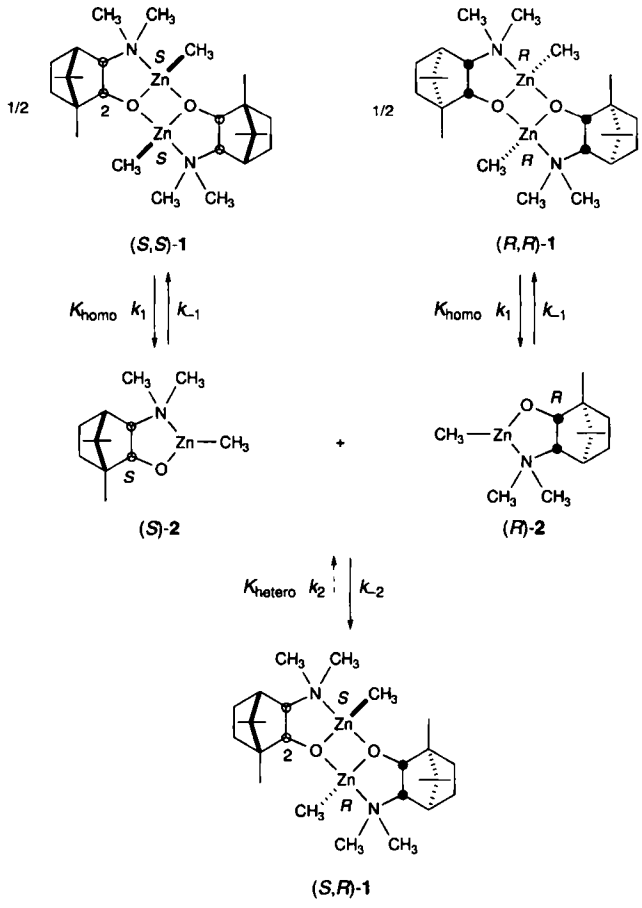

Scheme 2. Homochiral and heterochiral interaction of enantiomeric methylzinc aminoalkoxides. $K_{homo} = k_1/k_{-1} \approx 3 \times 10^{-2}$; $K_{hetero} = k_2/k_{-2} \approx 1 \times 10^{-5}$ (toluene, 40 °C).

Abstract in Japanese:

樟脳から誘導される(2*S*)-あるいは(2*R*)-3-*exo*-(ジメチルアミノ)イソボルネオール[(2*S*)-あるいは(2*R*)-DAIB]はジメチル亜鉛と反応して、メタンの発生とともに、対応するメチル亜鉛アミノアルコキシドとなる。この不斉な不飽和三配位有機亜鉛錯体は二量化して安定化する。この際、同じキラリティーをもつ単量体が自己相互作用するとS,Sあるいは*R*,*R*の不斉な二核亜鉛錯体が、また、反対のキラリティーをもつものが非自己相互作用するとメソ型の二量体が生じる。溶液中でも結晶中でも、ヘテロキラル二量体がホモキラル二量体に比較して圧倒的に安定であり、この相違が、DAIB-Zn錯体を触媒に用いるアルデヒド類に対する有機亜鉛化合物のエナンチオ選択的付加反応において不斉増幅現象を惹き起こす根源となる。核磁気共鳴スペクトルや分子量測定から、ホモキラル二量体はヘテロキラル二量体よりも単量体に解離しやすく、また窒素-亜鉛結合の解離、回転、再結合も容易に起こることがわかる。この動的挙動の相違は結晶構造の比較からも理解できる。S,S二量体のZn-OおよびZn-N結合はS,R体よりも長い。多環性骨格の空間的な混み合いが主な原因であり、立体的および電子的要因がその程度を支配する。ホモキラル二量体におけるC-2位水素原子と相手側のDAIBのN-メチル水素間の距離は、立体反発の結果、ファンデルワールス半径の和に近い。溶液中でも大きな核オーバーハウザー効果が観測される。二量体において四配位構造をもつ亜鉛原子は、メチル基とは共有結合、二つの酸素原子とは共有結合と静電的相互作用の混成結合、ジメチルアミノ基とは静電的相互作用を介して結びついている。ホモキラル二量体においては1,3シン配置の二つのZn-CH_3結合の電子が反発することも、不安定化の要因となっている。さらに、ホモキラル二量体では、酸素原子と亜鉛原子間の静電的相互作用が強められるためにN-Zn相互作用が弱くなることがわかる。これらの考察は非経験的分子軌道計算によっても支持される。

Results and Discussion

Solution-Phase Behavior: ^{1}H NMR spectra of (*S*,*R*)-**1** and (*S*,*S*)-**1** taken in [D$_8$]toluene revealed the contrasting dynamic behavior of the stereoisomers in solution.

Skeletal Congestion: An obvious structural difference between the diastereomeric compounds is the extent of skeletal congestion. In the *syn*-configurated homochiral dimer (*S*,*S*)-**1** the proximity of the C-2 proton of the DAIB skeleton and an *N*-methyl group in the other DAIB unit is suggested by the molecular model as well as the crystal structure (see below). Its 12 mM [D$_8$]toluene solution exhibited a 13% nuclear Overhauser effect (NOE) at room temperature (Fig. 1a). With heterochiral (*S*,*R*)-**1**, the C-2 proton is close to the Zn-CH_3 group in the enantiomeric organozinc moiety, exhibiting 7% NOE at room temperature in a 12 mM [D$_8$]toluene solution (Fig. 1b).

Dimer-Monomer Equilibration: The spectrum of a 10 mM [D$_8$]toluene solution of the heterochiral dimer (*S*,*R*)-**1** at 25 °C exhibited a single sharp *Zn*-methyl singlet at $\delta = -0.28$ and two distinct *N*-methyl singlets at $\delta = 2.26$ and 2.46, consistent with the *meso* structure. The spectrum was essentially temperature-independent in a range of 0 to 80 °C (Fig. 1b). The low solubility of (*S*,*R*)-**1** did not allow measurement at lower temperatures. The *Zn*-methyl and *N*-methyl signals remained sharp, while the chemical shift drifted by −0.10 and by +0.02–0.07 ppm, respectively, from 25 to 80 °C. Thus the heterochiral dimer appears to be very stable in toluene solution.

0947-6539/96/0209-1174 $ 15.00+.25/0 Chem. Eur. J. 1996, 2, No. 9

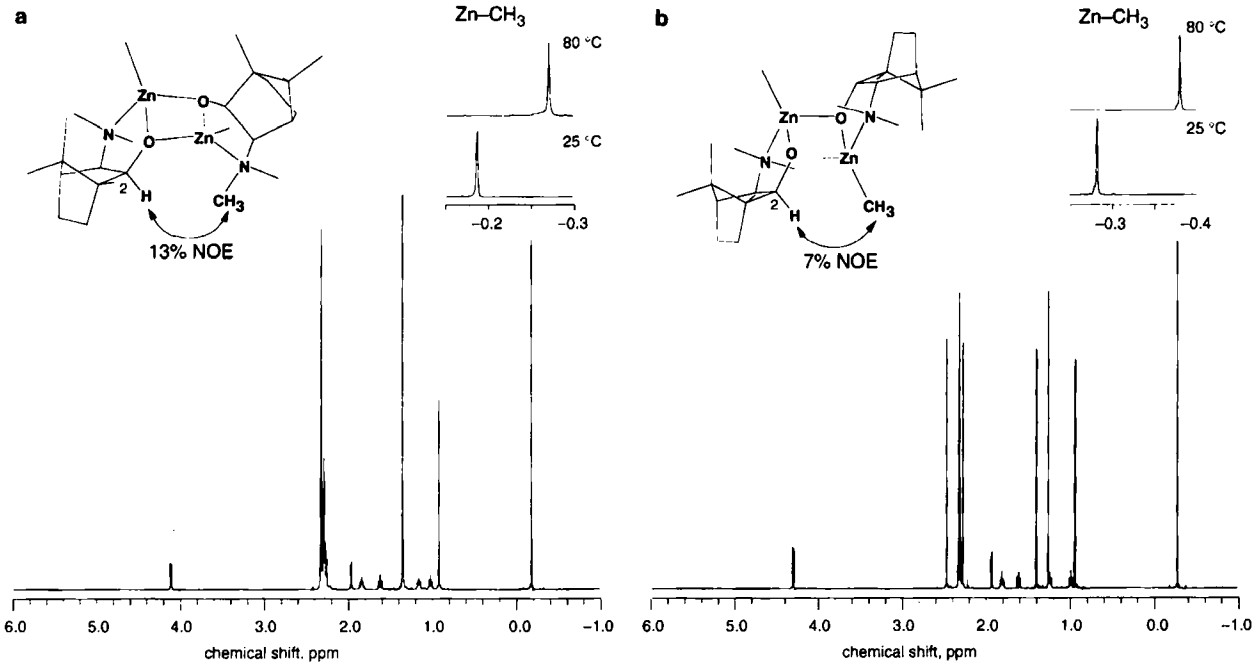

Fig. 1. ^{1}H NMR spectra of a) (*S,S*)-**1** and b) (*S,R*)-**1** in [D_8]toluene (10 mM) at 25 °C with the expanded signals of *Zn*-methyl protons at 25 and 80 °C.

The NMR behavior of the homochiral dimer (*S,S*)-**1** is entirely different (Fig. 1a). Its 10 mM [D_8]toluene solution at −40 °C gave a *Zn*-methyl singlet at $\delta = -0.05$ and two *N*-methyl singlets at $\delta = 2.18$ and 2.23. At 25 °C, however, owing to the fact that (*S,S*)-**1** dissociates to the monomer more readily than (*S,R*)-**1**, the *Zn*-methyl signal of (*S,S*)-**1** became broader than that of (*S,R*)-**1** (2 Hz vs. 1 Hz). Thus the time-averaged NMR spectra suggest that the dimer–monomer equilibration, (*S,S*)-**1**⇌2(*S*)-**2**, cannot be frozen at room temperature. Heating the solution to 80 °C gave a sharp *Zn*-methyl signal with a half-width of 1 Hz. The signal shifted from $\delta = -0.05$ (−40 °C) to $\delta = -0.19$ (25 °C) to $\delta = -0.27$ (80 °C). In addition, above 25 °C, the signal of the *N*-methyl groups in (*S,S*)-**1** became a singlet at $\delta = 2.28$ owing to topomerization, which will be discussed below.

Both homochiral and heterochiral **1** have dinuclear interactions in toluene solution, but the stability of the dimer differs. Notably, mixtures of dimethylzinc and (2*S*)-DAIB of various enantiomeric purities appear to exhibit two sets of ^{1}H NMR signals in a ratio corresponding to the resulting diastereomeric dimers, (*S,S*)- and (*S,R*)-**1**, instead of the monomers, (*S*)- and (*R*)-**2**. Because of the overwhelming stability of the heterochiral dimer, use of an *n*:1 mixture of (2*S*)- and (2*R*)-DAIB ($n > 1$) resulted in a pair of signals in an $(n-1)/2:1$ ratio rather than an *n*:1 ratio. The mole ratio of (2*S*)- and (2*R*)-DAIB determined the signal intensities of the homochiral and heterochiral "dimers", but did not influence the chemical shifts. These observations indicate that the equilibration of Scheme 2 is not rapid on the NMR timescale. The homochiral dimer (*S,S*)-**1** must be equilibrating with the monomer (*S*)-**2**. However, the ^{1}H NMR of (*S,S*)-**1** displayed only time-averaged spectra at 80 to −40 °C; no monomeric species **2** could be detected as an independent entity, even at low temperatures. Based on the vapor pressure osmometry measurements, the homochiral dimer and monomer were estimated to be present in a ca. 2:1 ratio in a 4–6 mM toluene solution at 40 °C.[11] Thus we can conclude that heterochiral (*S,R*)-**1** exists mostly as the dimer in toluene and dissociates to the monomeric species very slowly on the NMR timescale, while the homochiral isomers (*S,S*)- and (*R,R*)-**1** are in equilibrium with the monomeric species **2**. The spectrum is actually due to a mixture of stable (*S,R*)-**1** and labile (*S,S*)-**1** equilibrating with (*S*)-**2**.

Topomerization of the N-Methyl Groups: In addition to the dissociation into the monomer, the homochiral dimer exhibits an interesting intramolecular dynamic change, illustrated in Scheme 3. Although the dimethylamino moiety in (*S,S*)-**1** is definitely bound to Zn in the crystalline state, as will be discussed below, the dimer in toluene is in equilibrium with the tricoordinate complex (*S,S*)-**3**, in which an N–Zn bond is ruptured, while the central Zn_2O_2 four-membered ring is intact. The averaging process takes place by dissociation of the dimethylamino moiety from Zn, rotation about the N–C3 bond, configurational flipping at the nitrogen (or vice versa),

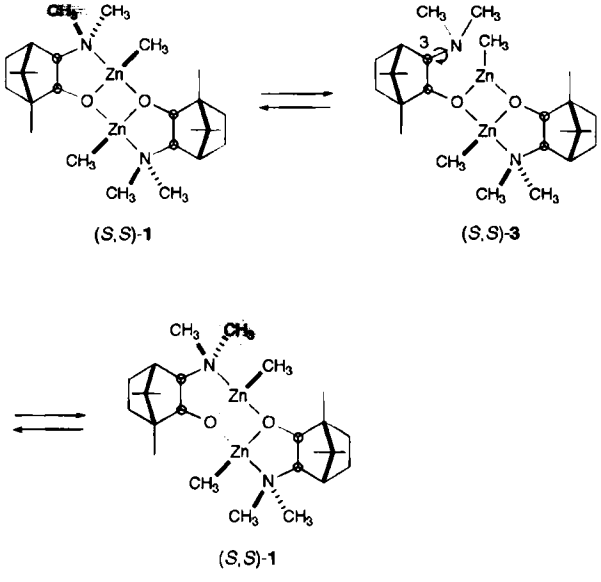

Scheme 3. Topomerization of *N*-methyl groups in (*S,S*)-**1**.

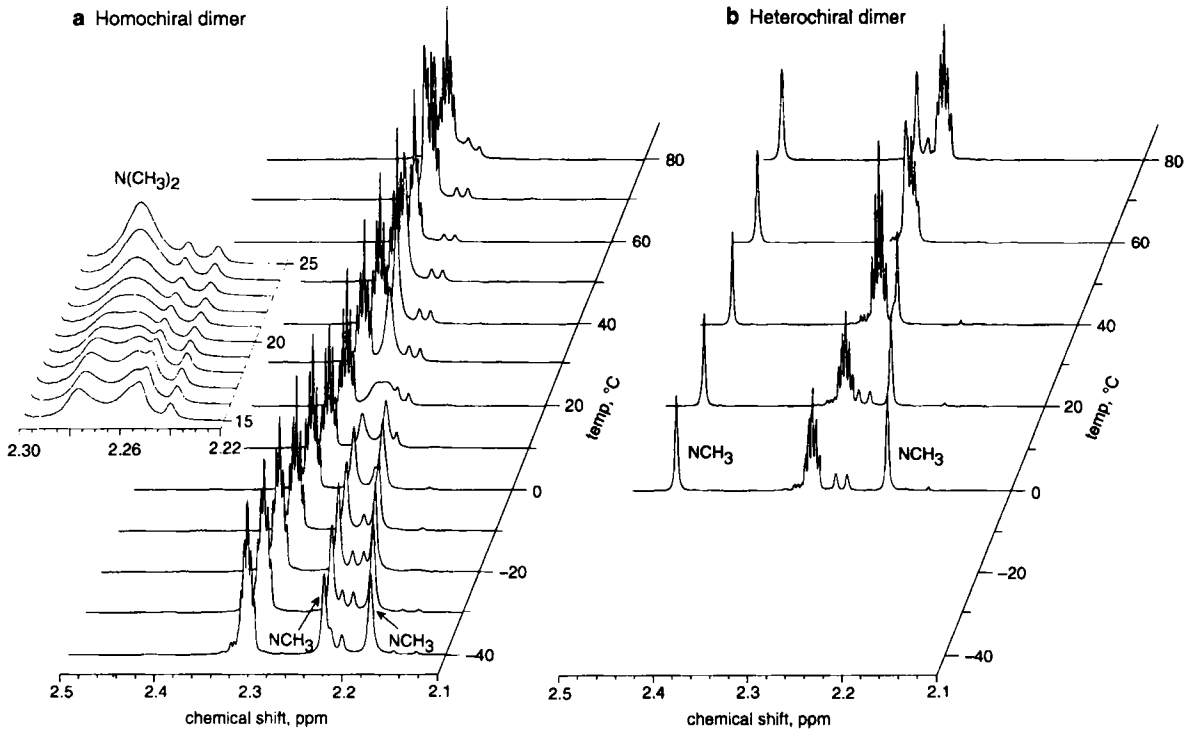

Fig. 2. Variable-temperature 600 MHz ^{1}H NMR spectra of a 10 mM solution of a) (*S,S*)-**1** and b) (*S,R*)-**1** in [D_8]toluene.

and coordination to Zn. This mechanism is substantiated by the variable-temperature ^{1}H NMR spectra of (*S,S*)-**1** taken with a 600 MHz instrument, which showed the two *N*-methyl groups to be magnetically equivalent above room temperature (Fig. 2a). The signal coalesced at 21 °C, and base-line separation of the two signals was attained only below 0 °C. The signals shifted upfield by 0.12 ppm from 80 to −40 °C. The standard line-shape analysis[14] indicated that the loss of nitrogen chirality occurs with an activation energy of 61 kJ mol^{-1}. Although the topomerization of Scheme 3 occurs in four steps, the initial dissociation of the amine ligand is the rate-limiting process and detectable by NMR. The other three steps are low-energy processes.[15, 16] The solute concentration in a 1–10 mM range did not affect the coalescence temperature in accordance with the maintenance of the dinuclear interaction during the intramolecular exchange reaction.[17–19] The heterochiral dimer (*S,R*)-**1** did not show an intramolecular exchange in a 0–80 °C temperature range; two distinct *N*-methyl signals were observed in the NMR spectrum (Fig. 2b).

Crystal Structures: The marked differences in the solution behavior between the diastereomeric dimers are reflected in their crystal structures. Calorimetric analysis has revealed that heterochiral (*S,R*)-**1** is more stable than homochiral (*S,S*)-**1** by 3.4 kJ mol^{-1} in the crystalline state.[11] The molecular structures of (*S,S*)-**1** and (*S,R*)-**1**, determined by single-crystal X-ray analysis, are illustrated in Figure 3.[6c, 20] The dinuclear Zn complexes contain two tetracoordinate Zn atoms with N–Zn dative bonds and two tricoordinate oxygen atoms in the central Zn_2O_2 four-membered ring. The Zn(1)–O(1) and Zn(2)–O(2) bonds are present in the monomer **2**, whereas the Zn(1)–O(2) and Zn(2)–O(1) linkages are created in the electro-complementary dimerization.

Although the stereoisomers (*S,S*)-**1** and (*S,R*)-**1** have a number of common structural features, they display several notable differences. The most significant is in the structure of the central Zn_2O_2 four-membered ring. The "dimer-forming" Zn(1)–O(2) and Zn(2)–O(1) bonds in (*S,S*)-**1** are longer than in (*S,R*)-**1** (2.05 vs. 2.028 Å), whereas the "internal" Zn(1)–O(1) and Zn(2)–O(2) bonds are shorter in the homochiral isomer (1.98 vs. 2.001 Å). The dimer structures are stabilized to different extents by the covalent and dative bonding contributions of these Zn–O bonds.[3a, 21] The Zn(1)–O(2) and Zn(1)–O(1) distances in (*S,R*)-**1** differ by only 1.3% (2.028 vs. 2.001 Å), while, in (*S,S*)-**1**, the Zn(1)–O(2) bond is 4% longer than Zn(1)–O(1) (2.05 vs. 1.98 Å). This inequality, which reflects the extent of the electron delocalization, is consistent with the weaker dimeric interaction in the homochiral dimer.

A second difference is in the conformations of the Zn_2O_2 rings in the diastereomers. The four-membered skeleton in (*S,R*)-**1** is completely planar, while that in the (*S,S*) isomer possesses a highly puckered conformation. In other words, the oxygen atoms in (*S,R*)-**1** are pyramidal, whereas the oxygens of (*S,S*)-**1** have essentially flat structures, as illustrated by the sum of the three bond angles, namely, 330.4° (heterochial) vs. 347.2 and 341.0° (homochiral).

An additional difference is in the Zn–N distances. The dative bonds in (*S,S*)-**1** are 1.0–3.8% longer than in (*S,R*)-**1** (2.19–2.25 vs. 2.168 Å). This is consistent with the dynamic behavior of (*S,S*)-**1** in toluene, that is, the rapid topomerization of the *N*-methyl groups (Scheme 3).

The difference in stability between the diastereomeric dimers correlates with the relative skeletal congestion of the central 5/4/5-fused tricyclic skeletons (Fig. 3). The heterochiral dimer, (*S,R*)-**1**, with C_i symmetry possesses an *anti* geometry, which is favored over the *syn* framework of the C_2 homochiral dimer, (*S,S*)-**1**. Owing to the higher skeletal congestion in (*S,S*)-**1**, its Zn(1)-O(2)-C-2′ and Zn(2)-O(1)-C-2 angles (average 128°) and N(1)-Zn(1)-O(2) and N(2)-Zn(2)-O(1) angles (average 118.8°) are substantially larger than those in (*S,R*)-**1** (116.0 and 111.0°, respectively). The spatial proximity of the bornane C-2 *endo* proton and one of the *N*-methyl groups in (*S,S*)-**1** induces dis-

0947-6539/96/0209-1176 $ 15.00+.25/0 Chem. Eur. J. 1996, 2, No. 9

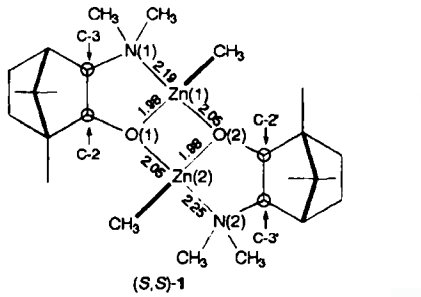

(*S*,*S*)-**1**

total valence angle at O(1) and O(2): 347.2° and 341.0°
Zn(1)–O(2)–C-2' and Zn(2)–O(1)–C-2: 130.0° and 126.0°
N(1)–Zn(1)–O(2) and N(2)–Zn(2)–O(1): 116.9° and 120.6°
CH_3–Zn(1)–O(2) and CH_3–Zn(2)–O(1): 117.6° and 116.0°

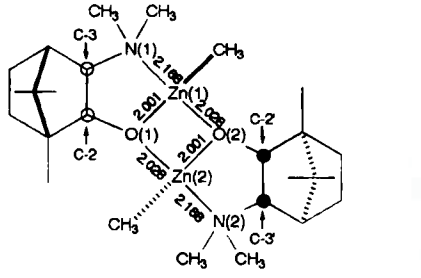

(*S*,*R*)-**1**

total valence angle at O(1) and O(2): 330.4°
Zn(1)–O(2)–C-2' and Zn(2)–O(1)–C-2: 116.0°
N(1)–Zn(1)–O(2) and N(2)–Zn(2)–O(1): 111.0°
CH_3–Zn(1)–O(2) and CH_3–Zn(2)–O(1): 116.1°

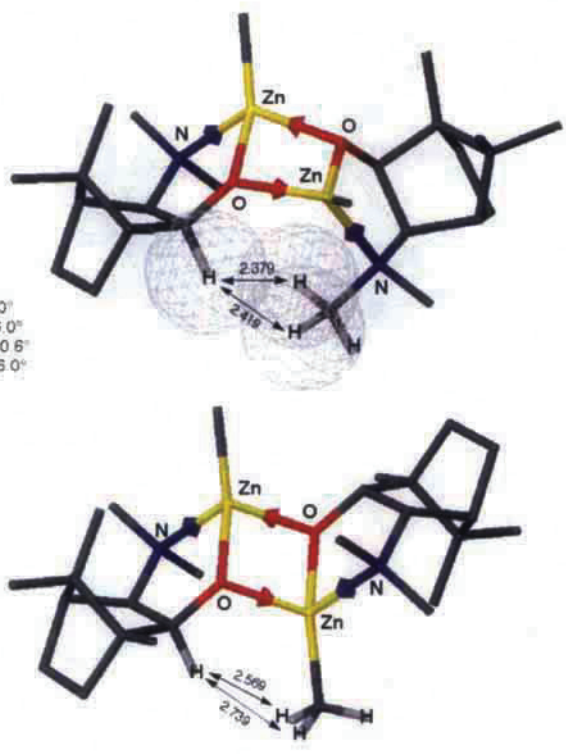

Fig. 3. Molecular structures of (*S*,*S*)-**1** and (*S*,*R*)-**1** determined by single-crystal X-ray analysis. The H···H distances are estimated by MO calculations. Note that the van der Waals surfaces of the hydrogens touch in (*S*,*S*)-**1** in the crystalline state.

tortion of the whole structure, which mitigates the nonbonding repulsion. In fact, the short H···H distances shown in Figure 3 (2.38 and 2.42 Å) are very close to the sum of the van der Waals radii (2.4 Å). The puckering of the Zn_2O_2 plane in the *syn* geometry somewhat relieves these steric interactions, but increases tortional and angular strain in the 5/4/5 tricycle. Overall, the structural modification is incapable of overcoming the instability of (*S*,*S*)-**1**. In contrast, in (*S*,*R*)-**1**, the C-2 proton is close to the *Zn*-methyl group, but the shortest H···H distance (2.57 Å) is too long to cause nonbonding repulsion.

Electronic and Steric Effects on the Structures: The homochiral dimer of (*S*)- or (*R*)-**2** is less stable than the heterochiral isomer, both in solution and in the crystalline state.[22] The solid-state structures provide explanations for the solution-phase properties, since bond length is one of the most useful probes of intramolecular environments. The Zn(1)–O(2) and Zn(2)–O(1) distances in (*S*,*S*)-**1** are longer than those in (*S*,*R*)-**1** (Fig. 3), in line with the relative stabilities of these stereoisomers. In addition, the N–Zn dative bonds in (*S*,*S*)-**1** are substantially longer than the corresponding linkages in (*S*,*R*)-**1**, consistent with the lability of the dative bonds of the former in toluene. Thus, the X-ray crystallographic analyses offer precise information on the structures of the stable, crystalline Zn complexes **1**, which correlates with the information on the solution structures provided by the NMR spectra. The experimentally observed properties are a consequence of electronic and steric factors: the sterically demanding DAIB skeleton as well as the nitrogen substituents play a significant role in determining the molecular structures. Therefore, in addition to the spectroscopic and crystallographic data, a study of the molecular orbitals (MO) in simpler model systems should provide a more complete understanding of the structure-determining factors.

We performed ab initio MO calculations on the structurally less perturbed systems. The simple dinuclear complex **5** (dimer of **4**) and the *N*,*N*,*N*′,*N*′-tetramethyl analogue **7** (dimer of **6**) were selected as models of **1**. The absence of the bornane skeleton in both **5** and **7** is reflected in the twist angles around the C(1)–C(2) and C(4)–C(5) bonds in **5** and around the C(1)–C(2) and C(6)–C(7) bonds in **7**. The *N*-methyl groups do not affect the monomer structures **4** and **6**, but exert a profound influence on the geometries of the dimers **5** and **7**, mainly for steric reasons. Figures 4 and 5 illustrate the calculated structures of the organozinc complexes **4**–**7**. Total energies of the compounds are listed in Table 1. The relative energies are corrected with ZPE. Formation of *syn*-**5** and *anti*-**5** from the monomer **4** is exothermic by 144.4 kJ mol^{-1} (72.2 kJ per mol of **4**) and 161.3 kJ mol^{-1} (80.6 kJ per mol of **4**), respectively. The dimerization of the *N*-methylated compound **6** to give *syn*-**7** and *anti*-**7** is exothermic by 137.7 kJ mol^{-1} (68.9 kJ per mol of **6**) and 179.1 kJ mol^{-1} (89.5 kJ per mol **6**), respectively.

In going from compound **1** to the simplest model **5**, the electronic effects become more prominent. The calculated structures indicate significant electron delocalization in the central Zn_2O_2 four-membered rings. Like in the crystal structures of **1** (Fig. 3), *syn*-**5** has a puckered Zn_2O_2 ring, while *anti*-**5** possesses a planar geometry. This difference can therefore only partially be attributed to steric effects. The *syn* stereoisomer is more polar than the *anti* isomer; this results in more repulsions between bonding-pair electrons, which are alleviated in the nonplanar geometry. The greater sp^2 character of the oxygen atoms in the *syn* isomer is indicated by calculation: the sum of the three bond angles for the *syn* and *anti* isomer are 348.2 and 340.4°, respectively. This structural feature of the *syn* isomer is associated with electronic stabilization of the dinuclear structure. The oxygen atom with a p-like oxygen nonbonding orbital has electrostatic interactions with the neighboring Zn atoms; this effect is weaker in the *anti* isomer with sp^3-like nonbonding orbitals at O. It should be noted that the Zn atom cannot form a π bond by interacting with the oxygen p orbital since the 4s orbital is vacant.[13] This electrostatic attraction results in a 0.4% shortening of the Zn(1)–O(2) and Zn(2)–O(1) bond of *syn*-**5** with respect to the corresponding bonds in *anti*-**5** (1.979 vs. 1.985 Å; Fig. 4). The internal Zn(1)–O(1) and Zn(2)–O(2) bonds, as well as the Zn–CH_3 bonds, are comparable. This oxygen-to-Zn electron-releasing effect in *syn*-**5** increases the Zn–N distances relative to those in *anti*-**5** (2.308 vs. 2.250 Å; 2.6% difference).[23, 24]

The C–Zn bond in *syn*-**5** is highly polar: the calculated charges at C and Zn are −1.0700 and +1.5233, respectively (Table 2). The negative charge at the carbon atom is even larger than at the nitrogen atom (−0.9594). The *anti* isomer has a

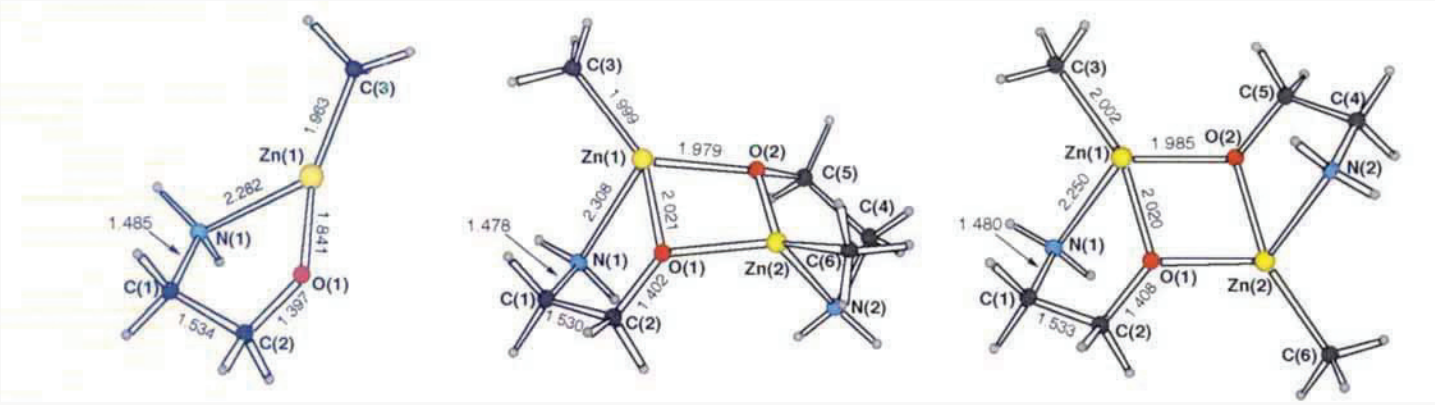

total valence angle at O(1) and O(2): 348.2°
Zn(1)–O(2)–C(5) and Zn(2)–O(1)–C(2): 132.9°
N(1)–Zn(1)–O(2) and N(2)–Zn(2)–O(1): 110.7°
C(3)–Zn(1)–O(2) and C(6)–Zn(2)–O(1): 130.8°

total valence angle at O(1) and O(2): 340.4°
Zn(1)–O(2)–C(5) and Zn(2)–O(1)–C(2): 125.5°
N(1)–Zn(1)–O(2) and N(2)–Zn(2)–O(1): 111.3°
C(3)–Zn(1)–O(2) and C(6)–Zn(2)–O(1): 126.4°

Fig. 4. Calculated structures of **4**, *syn*-**5**, and *anti*-**5**.

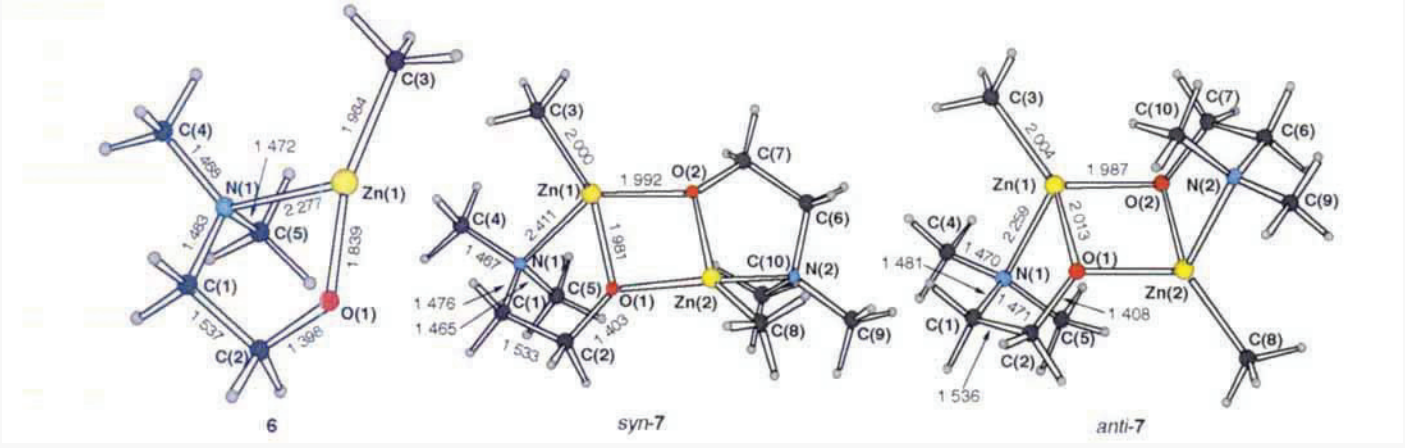

total valence angle at O(1) and O(2): 358.1°
Zn(1)–O(2)–C(7) and Zn(2)–O(1)–C(2): 138.7°
N(1)–Zn(1)–O(2) and N(2)–Zn(2)–O(1): 124.0°
C(3)–Zn(1)–O(2) and C(8)–Zn(2)–O(1): 123.1°

total valence angle at O(1) and O(2): 341.8°
Zn(1)–O(2)–C(7) and Zn(2)–O(1)–C(2): 127.0°
N(1)–Zn(1)–O(2) and N(2)–Zn(2)–O(1): 111.7°
C(3)–Zn(1)–O(2) and C(8)–Zn(2)–O(1): 125.1°

Fig. 5. Calculated structures of **6**, *syn*-**7**, and *anti*-**7**.

Table 1. Total energies and zero-point energies (ZPE) for **4**–**9** (in hartrees).

	RHF//HRF	ZPE [a]	RMP2//RHF
4	− 2025.7150	0.1337	− 2026.9087
syn-**5**	− 4051.5003	0.2685	− 4053.8734
anti-**5**	− 4051.5056	0.2691	− 4053.8804
6	− 2103.7302	0.1932	− 2105.2590
syn-**7**	− 4207.5277	0.3882	− 4210.5723
anti-**7**	− 4207.5376	0.3887	− 4210.5885
8	− 4207.5229	0.3873	− 4210.5631
9	− 2103.7096	0.1921	− 2105.2295

[a] The zero-point energies are from the RHF frequency calculations.

Table 2. Mulliken bond populations and atomic charges (*e*) for **4**–**7**.

	4	*syn*-**5**	*anti*-**5**	**6**	*syn*-**7**	*anti*-**7**
bond population						
Zn(1)–O(1)	0.0792	0.0211	0.0218	0.0783	0.0270	0.0215
Zn(1)–N(1)	−0.0069	−0.0049	0.0008	−0.0101	0.0051	0.0082
Zn(1)–C(3)	0.2139	0.2176	0.2099	0.2154	0.2131	0.2067
C(1)–N(1)	0.1015	0.1276	0.1201	0.1038	0.1390	0.1210
C(1)–C(2)	0.2599	0.2813	0.2729	0.2583	0.2859	0.2733
O(1)–C(2)	0.1959	0.1527	0.1444	0.1907	0.1375	0.1345
Zn(1)–O(2)	–	0.0216	0.0233	–	0.0119	0.0201
N(1)–C(4)	–	–	–	0.1535	0.1644	0.1517
N(1)–C(5)	–	–	–	0.1408	0.1611	0.1395
atomic charge						
Zn(1)	1.4264	1.5233	1.5291	1.4314	1.5282	1.5412
O(1)	−1.0350	−1.1375	−1.1364	−1.0410	−1.1544	−1.1393
N(1)	−0.9922	−0.9594	−0.9767	−0.8423	−0.7841	−0.8347
C(1)	−0.1611	−0.1657	−0.1653	−0.1403	−0.1405	−0.1395
C(2)	0.1308	0.1410	0.1203	0.1248	0.1313	0.1097
C(3)	−1.0880	−1.0700	−1.0748	−1.0856	−1.0650	−1.0737
C(4)	–	–	–	−0.2300	−0.2290	−0.2322
C(5)	–	–	–	−0.2623	−0.2486	−0.2353

similar charge distribution. The Mulliken population analysis indicates that the Zn atoms in **5** are bound to the neighboring atoms in three different ways, shown schematically in Figure 6. The Zn–CH_3 linkage is a covalent bond, while the Zn–O bonds are hybrids of a covalent and, predominantly, electrostatic bond.[3d] Notably, the Zn–N interaction is highly electrostatic in nature and has a negligible covalent character, as indicated by the very small bond population.[4a, 13] The inherent electron deficiency at the Zn^{II} atoms is further compensated by the donation of nonbonding electrons from the oxygen atoms. The extent of this effect is strongly affected by the hybridization of the oxygen atoms and, accordingly, marked differences are seen between the stereoisomers. The N-to-Zn donation, in addition to the Zn_2O_2 sigma framework, is the major Coulombic term

© VCH Verlagsgesellschaft mbH, D-69451 Weinheim, 1996 0947-6539/96/0209-1178 $ 15.00+.25/0 Chem. Eur. J. 1996, 2, No. 9

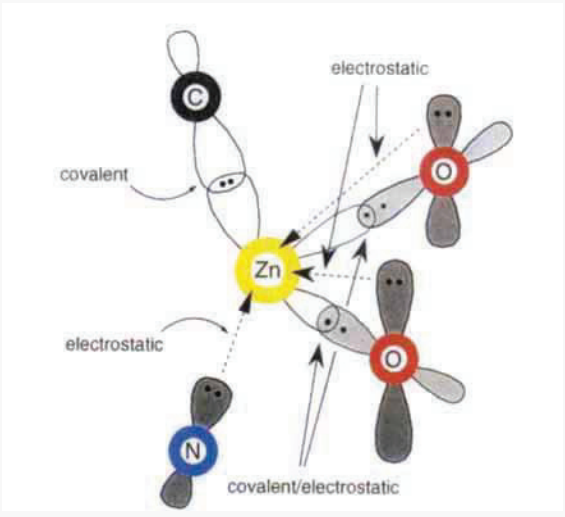

Fig. 6. Nature of bonding in the tetracoordinated Zn complex.

neutralizing the electron-deficient Zn^{II} centers of *anti*-**5**, while the both N–Zn and O–Zn interactions cooperate in the stabilizing the *syn* isomer (Fig. 6). In fact, in spite of the shortness of the Zn(1)–O(2) (and Zn(2)–O(1)) bond of *syn*-**5** relative to that of *anti*-**5**, the population is slightly smaller.

The electronic model **5** has no *N*-methyl groups and thus does not suffer from any nonbonding repulsion between the substituents. Consequently, unlike the real complexes **1**, the dimer-forming Zn–O bonds in *syn*-**5** are shorter than those in *anti*-**5**. Nevertheless, *syn*-**5** is less stable than *anti*-**5** by 16.9 kJ mol^{-1}. The instability of the *syn* stereoisomer must therefore be electronic in nature. In fact, the extent of repulsion between bonding-pair electrons has been found to be the major factor determining the relative stabilities of the stereoisomers. The *syn* stereoisomer possesses sets of C–Zn and N–Zn linkages, both oriented 1,3-*syn*. The MO correlation diagram illustrated in Figure 7 reveals that *syn*-**5** is destabilized primarily by the repulsion between the Zn–CH_3 bonding-pair electrons. The 71st, 70th, and 68th MOs of *syn*-**5** and *anti*-**5** exhibit the greatest energy differences. The 71st MOs (next HOMOs) are created by

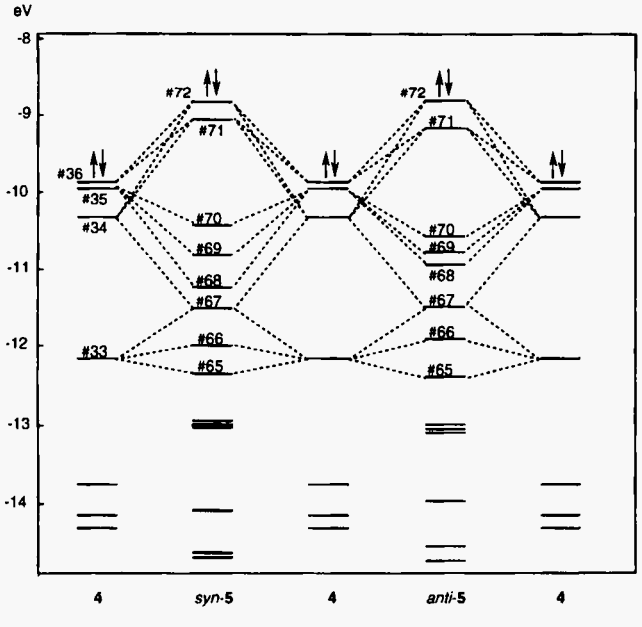

Fig. 7. MO diagrams for **4**, *syn*-**5**, and *anti*-**5**. The double arrows show the Fermi surface.

combining the Zn–CH_3 bonding orbitals of **4** in the same phase (Fig. 8), which lead to the destabilization of the *syn* isomer by electronic repulsion. The 70th and 68th MOs result from interaction of the nonbonding oxygen orbitals of **4**, which tend to stabilize *syn*-**5**. The polar Zn–N bonds contribute less to the stability difference.

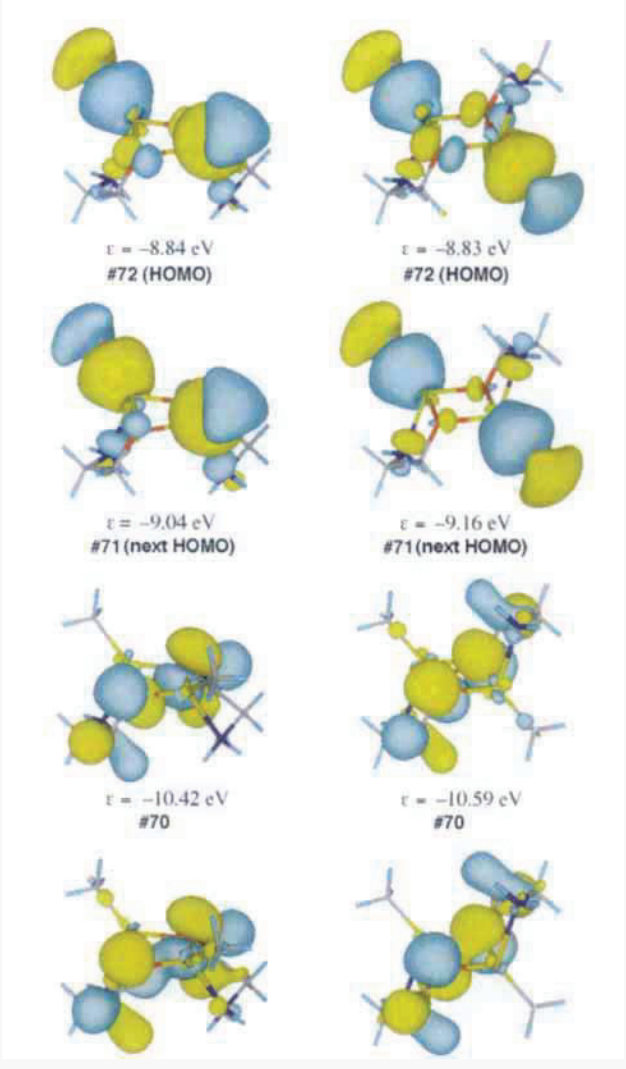

Fig. 8. Selected MOs of *syn*-**5** (left) and *anti*-**5** (right).

Steric factors are also significant. The calculation of the steric model **7** indicates that the *anti* isomer is more stable than the *syn* isomer by as much as 41.4 kJ mol^{-1}. In going from *syn*-**5** to the *N*-methylated compound *syn*-**7**, the Zn(1)–O(2) (and Zn(2)–O(1)) bond is considerably elongated from 1.979 to 1.992 Å (Figs. 4 and 5). In contrast to the electronic model **5**, this dimer-forming bond is now slightly longer than in *anti*-**7** (1.987 Å). In *syn*-**7**, the dimer-forming Zn–O bonds are longer than the internal Zn–O bonds, while the relative lengths are reversed in *anti*-**7**. Furthermore, the C(2)-O(1)-Zn(2) and C(7)-O(2)-Zn(1) angles in the *syn* isomer are larger than in *syn*-**5** (138.7 vs. 132.9°). The p character of the O(1) and O(2) atoms is also greatly increased from the simple model *syn*-**5** (sum of the the three bond angles, 348.2° (*syn*-**5**) vs. 358.1° (*syn*-**7**)), while the oxygens of *anti*-**7** remain substantially sp^3 in character (341.8°). Thus the electronic effects tend to shorten the dimer-forming

Zn–O bonds, but the steric effects of the *N*-methyl groups actually result in bond elongation.

N-Methylation slightly affects the electronic nature of the N–Zn linkage of the organozinc compounds (Table 2). The electronic repulsion of the 1,3-*syn*-CH_3–Zn bonds contributes to the instability of *syn*-**7**. All the differences between **5** and **7** are due to the absence or presence of sterically demanding *N*-methyl groups, and the majority of the geometrical features of **7** are correlated to the real compounds **1**. It should be added, however, that the model **7**, which lacks the bornane skeletons, is still structurally more relaxed than the real system **1**. For example, *syn*-**7** no longer suffers C(2)–*H*/C(10)–*H* nonbonded repulsion (3.89–4.02 Å); the shortest distance is N(1)$CH_3\cdots$N(2)CH_3 (2.47 Å).

Notably, the dimer forming Zn–O bond in *syn*-**7** is more ionic than in *anti*-**7**, which is most clearly reflected in the smaller bond population relative to that of the inner Zn–O bond (*syn*-**7**, 0.0119 vs. 0.0270; *anti*-**7**, 0.0201 vs. 0.0215) (Table 2). A difference of this type is not seen in the non-methylated model **5**. Thus *N*-methylation of the *syn* isomer elongates the dimer-forming Zn–O linkages and also enhances the ionic character. Furthermore, the N–Zn bonds in *syn*-**7** are substantially longer than in *anti*-**7**, as was found in **5**. This is consistent with the ready averaging process of the *N*-methyl signals in the ^{1}H NMR of (*S*,*S*)-**1**, but not of (*S*,*R*)-**1** (Fig. 2). The MO calculation suggests that the bond-dissociated isomer **8** (model of (*S*,*S*)-**3** in Scheme 3; Fig. 9) is 21.9 kJ mol^{-1} less stable than *syn*-**7**. The monomer **6** can liberate the amino moiety, generating the linear dicoordinated species **9**, but with a higher endothermicity (ΔE = 74.6 kJ mol^{-1}).

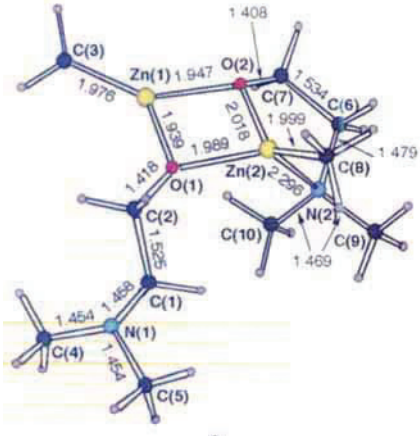

8

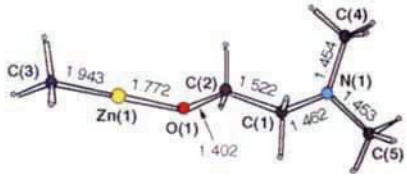

9

total valence angle at O(1) and O(2): 358.2° and 347.3°
Zn(1)–O(2)–C(7) and Zn(2)–O(1)–C(2): 132.0° and 128.9°
N(2)–Zn(2)–O(1): 111.1°
C(3)–Zn(1)–O(2) and C(8)–Zn(2)–O(1): 138.1° and 127.3°

Fig. 9. Calculated structures of **8** and **9**.

Thus the study of the solution and crystal structures of **1** and the MO calculations on the model systems **5** and **7** have clarified differences in the properties between the *syn* and *anti* dimeric compounds. The marked differences can be understood in terms of steric and electronic factors. The *syn* 5/4/5 tricyclic system, even without additional steric constraints, is less stable than the *anti* stereoisomer for electronic reasons. In addition, nonbonded repulsion induced by the *syn*-configurated DAIB skeletons significantly increases the difference in the relative stabilities. The puckering of the central Zn_2O_2 skeleton of the *syn* isomer tends to reduce the unfavorable steric and electronic factors, but is unable to overcome the instability relative to the *anti* isomer.

Conclusion

The structures of the homochiral and heterochiral dinuclear Zn complexes **1**, formed from (2*S*)- or (2*R*)-3-*exo*-(dimethylamino)isoborneol and dimethylzinc, are distinctly different, and this can be used to rationalize the chirality amplification, which has been observed in the asymmetric reaction of dimethylzinc and benzaldehyde in the presence of small amounts of these Zn complexes.[6–8] The diastereomers (*S*,*S*)-**1**, (*R*,*R*)-**1**, and (*S*,*R*)-**1** all possess central Zn_2O_2 four-membered rings. The homochiral dimers are characterized by a *syn*-configurated 5/4/5 tricyclic skeleton, and the heterochiral isomer by an *anti* 5/4/5 framework. In both the solution and solid phase, the heterochiral dimer is more stable than the homochiral isomer. The crystal structures and behavior in toluene solution correlate well with one another. In the crystalline state, the dimer-forming Zn–O bonds as well as the N–Zn dative (electrostatic) bonds in homochiral **1** are longer than those in heterochiral **1**. The relative lengths of these bonds are reflected in their lability in toluene solution. The homochiral dimer dissociates easily into the monomer **2** and also undergoes ready topomerization of the *N*-methyl groups. The three-dimensional structures of the dinuclear complexes are subtly affected by both steric and electronic factors. MO calculations have elucidated the nature of bonding in the tetrahedral Zn complexes. The repulsion between the bonding-pair electrons of the 1,3-*syn*-oriented C–Zn bonds is the major factor destabilizing the *syn* isomer. Electronic effects tend to shorten the dimer-forming Zn–O bonds in the homochiral **1**, while the prevailing steric factors provide the opposite perturbation.

Experimental and Computational Procedure

Variable-Temperature NMR Studies: The homochiral and heterochiral dimers were synthesized by the reported method [6c]. The samples for the NMR measurements were prepared very carefully to avoid moisture and air, which decompose the organozinc complexes. Dimers (*S*,*S*)-**1** and/or (*S*,*R*)-**1** (5–10 mg) were weighed with the balance in a glove box filled with argon with a dew point of −95 °C. The sample was placed in a dry 5 mm NMR tube with a Teflon needle valve. The sealed NMR tube was taken out of the glove box and equipped, under an argon stream, with a Schlenk adapter connected to a vacuum–argon double-manifold line. [D_8]Toluene, distilled over a sodium/potassium alloy, was introduced into the NMR tube by use of a Teflon cannula under a slightly positive pressure of argon. The resulting solution was cooled to −78 °C, and the needle valve of the NMR tube was closed under reduced pressure. The NMR measurements were performed on a pulse FT NMR spectrometer JEOL JNM-A 600 (600 MHz ^{1}H frequency) equipped with an NM-AVT3 variable-temperature unit. The accuracy of the sample temperatures was ±1 °C, and no temperature corrections were applied to the data. Typical spectral parameters were as follows: spectral digitization, frequency = 8000 Hz, data point = 16 K; pulse width = 45° (6 μs); acquisition time = 2.0480 s; pulse delay = 3.9504 s; delay and dead time = 122 μs. Variable-temperature experiments for (*S*,*S*)-**1** were carried out over a temperature range from −40 to 80 °C. The temperature was raised in 10 °C steps from −40 to 10 °C and from 30 to 80 °C, and 1 °C steps from 15 °C to 25 °C. The spectra of (*S*,*R*)-**1** were measured at intervals of 10 °C from 0 to 80 °C. The topomerization rate constant k of the *N*-methyl groups of (*S*,*S*)-**1** was calculated by Gutowsky-Holm equation [Eq. (1)], where $\delta\nu$ is the width

$$k = \frac{\pi\delta\nu}{\sqrt{2}} \quad (1)$$

of a given coalescence signal. Substitution of $\delta\nu$ = 45 Hz for the *N*-methyl signal at the coalescence temperature of 21 °C affords $k = 1 \times 10^2$ s^{-1}. With the Eyring's

0947-6539/96/0209-1180 $ 15.00+.25/0 Chem. Eur. J. 1996, 2, No. 9

method [26]; the energy barrier for flipping at the nitrogen center was calculated to be 60.7 kJ mol^{-1}.

Computational Details: The ab initio calculations on the organozinc compounds **4**–**9** were carried out with the GAUSSIAN 92 program [27] using an all electron [8s 5p 3d]/(14s 9p 5d) basis set [28] for Zn and 6-31 G for C, H, N, and O. For each structure a full optimization was performed at the restricted Hartree–Fock (RHF) level using energy gradient techniques. The energy determination was made using a restricted second-order Møller-Plesset (MP 2) perturbation calculation by changing 6-31 G to 6-31 G** on the resulting local minimum. The closest atom distances between the C-2 proton and *N*-methyl proton of (*S,S*)-**1** and between the C-2 proton and *Zn*-methyl proton of (*S,R*)-**1** were estimated from the minimized geometries, which were computed by semiempirical molecular orbital calculations using the MOPAC 6.0 package and the AM 1 Hamiltonian by rotating the N–CH_3 or Zn–CH_3 bond with fixed coordinates for all atoms except for *N*- and *Zn*-methyl protons.

Received: April 23, 1996 [F 358]

[1] For example, a) R. Noyori, *Asymmetric Catalysis in Organic Synthesis*, John Wiley, New York, **1994**, p. 378; b) *Catalytic Asymmetric Synthesis* (Ed.: I. Ojima), VCH, Weinheim, **1993**, p. 476; c) M. Nógrádi, *Stereoselective Synthesis*, VCH, Weinheim, **1987**, p. 368; d) B. Bosnich, *Asymmetric Catalysis*, Martinus Nijhoff, Dordrecht, **1986**, p. 160; d) *Asymmetric Synthesis, Vol. 5* (Ed.: J. D. Morrison), Academic Press, New York, **1985**, p. 391.

[2] For a pioneering X-ray crystallographic study on donor–acceptor interactions of Lewis acid/Lewis base pairs, see: P. Chakrabarti, J. D. Dunitz, *Helv. Chim. Acta* **1982**, *65*, 1482–1488.

[3] Reviews: a) S. Shambayati, S. L. Schreiber in *Comprehensive Organic Synthesis, Vol. 1, Chapt. 1.10* (Ed.: B. M. Trost), Pergamon Press, Oxford, **1991**, pp. 283–324; b) P. G. Williard in *Comprehensive Organic Synthesis, Vol.1, Chapt. 1.1* (Ed.: B. M. Trost), Pergamon Press, Oxford, **1991**, pp. 1–47; c) S. Shambayati, W. E. Crowe, S. L. Schreiber, *Angew. Chem. Int. Ed. Engl.* **1990**, *29*, 256–272; d) A. Haaland, *ibid.* **1989**, *28*, 992–1007.

[4] Theoretical treatments: a) V. Jonas, G. Frenking, M. T. Reetz, *J. Am. Chem. Soc.* **1994**, *116*, 8741–8753; b) E. D. Glendening, A. Streitwieser, *J. Chem. Phys.* **1994**, *100*, 2900–2909; c) T. A. Holme, T. N. Truong, *Chem. Phys. Lett.* **1993**, *215*, 53–57; d) M. W. Wong, K. B. Wiberg, *J. Am. Chem. Soc.* **1992**, *114*, 7527–7535; e) P. G. Jasien, *J. Phys. Chem.* **1992**, *96*, 9273–9278; f) B. W. Gung, M. A. Wolf, *J. Org. Chem.* **1992**, *57*, 1370–1375; g) V. Branchadell, A. Oliva, *J. Am. Chem. Soc.* **1991**, *113*, 4132–4136; h) A. E. Reed, L. A. Curtiss, F. Weinhold, *Chem. Rev.* **1988**, *88*, 899–926; i) R. F. W. Bader, *Acc. Chem. Res.* **1985**, *18*, 9; j) R. S. Drago, *Coord. Chem. Rev.* **1980**, *33*, 251–277.

[5] For reviews on Lewis acid catalyzed asymmetric reactions, see: a) U. Pindur, G. Otto, *Chem. Rev.* **1993**, *93*, 741–761; b) H. B. Kagan, O. Riant, *ibid.* **1992**, *92*, 1007–1019; c) K. Narasaka, *Synthesis* **1991**, 1–11; d) *Selectivities in Lewis Acid Promoted Reactions* (Ed.: D. Schinzer), Kluwer Academic Publishers, Dordrecht, **1989**, p. 331.

[6] a) M. Kitamura, S. Suga, K. Kawai, R. Noyori, *J. Am. Chem. Soc.* **1986**, *108*, 6071–6072; b) R. Noyori, S. Suga, K. Kawai, S. Okada, M. Kitamura, *Pure Appl. Chem.* **1988**, *60*, 1597–1606; c) M. Kitamura, S. Okada, S. Suga, R. Noyori, *J. Am. Chem. Soc.* **1989**, *111*, 4028–4036; d) R. Noyori, S. Suga, K. Kawai, S. Okada, M. Kitamura, N. Oguni, M. Hayashi, T. Kaneko, Y. Matsuda, *J. Organomet. Chem.* **1990**, *382*, 19–37; e) M. Kitamura, S. Suga, M. Niwa, R. Noyori, *J. Am. Chem. Soc.* **1995**, *117*, 4832–4842.

[7] Reviews: a) R. Noyori, M. Kitamura, *Angew. Chem. Int. Ed. Engl.* **1991**, *30*, 49–69; b) K. Soai, S. Niwa, *Chem. Rev.* **1992**, *92*, 833–856.

[8] N. Oguni, Y. Matsuda, T. Kaneko, *J. Am. Chem. Soc.* **1988**, *110*, 7877–7878.

[9] K. Soai, T. Shibata, H. Morioka, K. Choji, *Nature* **1995**, *378*, 767–768.

[10] First report on the nonlinear effect in asymmetric reactions: a) C. Puchot, O. Samuel, E. Duñach, S. Zhao, C. Agami, H. B. Kagan, *J. Am. Chem. Soc.* **1986**, *108*, 2353–2357; b) C. Agami, J. Levisalles, C. Puchot, *J. Chem. Soc. Chem. Commun.* **1985**, 441–442. Other asymmetric reactions showing nonlinear effect: c) S. Kobayashi, H. Ishitani, M. Araki, I. Hachiya, *Tetrahedron Lett.* **1994**, *35*, 6325–6328; d) M. Terada, K. Mikami, *J. Chem. Soc. Chem. Commun.* **1994**, 833–834; e) K. Mikami, Y. Motoyama, M. Terada, *J. Am. Chem. Soc.* **1994**, *116*, 2812–2820; f) Q.-L. Zhou, A. Pfaltz, *Tetrahedron* **1994**, *50*, 4467–4478; g) A. H. M. de Vries, J. F. G. A. Jansen, B. L. Feringa, *ibid.* **1994**, *50*, 4479–4491; h) H. Sasai, T. Suzuki, N. Itoh, M. Shibasaki, *Tetrahedron Lett.* **1993**, *34*, 851–854; i) G. E. Keck, D. Krishnamurthy, M. C. Grier, *J. Org. Chem.* **1993**, *58*, 6543–6544; j) D. A. Evans, S. G. Nelson, M. R. Gagné, A. R. Muci, *J. Am. Chem. Soc.* **1993**, *115*, 9800–9801; k) N. Komatsu, M. Hashizume, T. Sugita, S. Uemura, *J. Org. Chem.* **1993**, *58*, 4529–4533; l) K. Tanaka, J. Matsui, H. Suzuki, *J. Chem. Soc. Perkin Trans. 1* **1993**, 153–157; m) B. Rossiter, M. Eguchi, G. Miao, N. M. Swingle, A. E. Hernández, D. Vickers, E. Fluckiger, R. G. Patterson, K. V. Reddy, *Tetrahedron* **1993**, *49*, 965–986; n) C. Bolm, M. Ewald, M. Felder, *Chem. Ber.* **1992**, *125*, 1205–1215; o) M. Hayashi, T. Matsuda, N. Oguni, *J. Chem. Soc. Chem. Commun.* **1990**, 1364–1365; p) N. Iwasawa, Y. Hayashi, H. Sakurai, K. Narasaka, *Chem. Lett.* **1989**, 1581–1584.

[11] M. Kitamura, S. Suga, M. Niwa, R. Noyori, Z.-X. Zhai, H. Suga, *J. Phys. Chem.* **1994**, *98*, 12776–12781.

[12] J. Boersma in *Comprehensive Organometallic Chemistry, Vol. 2, Chapt. 16* (Eds.: G. Wilkinson, F. G. A. Stone, E. W. Abel), Pergamon Press, Oxford, **1982**, pp. 823–862.

[13] M. Yamakawa, R. Noyori, *J. Am. Chem. Soc.* **1995**, *117*, 6327–6335.

[14] M. Ōki, M. Ohira, *Bull. Chem. Soc. Jpn.* **1984**, *57*, 3117–3121.

[15] ^{1}H NMR spectrum of DAIB *O*-benzoate in [D_8]toluene displays a single *N*-methyl signal even at −40 °C.

[16] The free energies of nitrogen inversion are normally less than 30 kJ mol^{-1} at −80 °C. See: C. H. Bushweller, S. H. Fleischman, G. L. Grady, P. McGoff, C. D. Rithner, M. R. Whalon, J. G. Brennan, R. P. Marcantonio, R. P. Domingue, *J. Am. Chem. Soc.* **1982**, *104*, 6224–6236.

[17] a) P. A. van der Schaaf, E. Wissing, J. Boesma, W. J. J. Smeets, A. L. Spek, G. van Koten, *Organometallics* **1993**, *12*, 3624–3629; b) S. C. Goel, M. Y. Chiang, W. E. Buhro, *Inorg. Chem.* **1990**, *29*, 4646–4652; c) J. Dekker, J. Boesma, L. Fernholt, A. Haaland, A. L. Spek, *Organometallics* **1987**, *6*, 1202–1206.

[18] M. R. P. van Vliet, P. Buysingh, G. van Koten, K. Vrieze, B. Kojic-Prodic, A. L. Spek, *Organometallics* **1985**, *4*, 1701–1707.

[19] a) M. L. Sierra, S. J. de Mel, J. P. Oliver, *Organometallics* **1989**, *8*, 2486–2488; b) R. Kumar, M. L. Sierra, J. P. Oliver, *ibid.* **1994**, *13*, 4285–4293.

[20] The X-ray crystallographic analysis of (*S,S*)- and (*S,R*)-**1** at −30 °C qualitatively showed the bond lengths and angles to be the same as those obtained at room temperature [6c].

[21] M. M. Olmstead, P. P. Power, S. C. Shoner, *J. Am. Chem. Soc.* **1991**, *113*, 3379–3385.

[22] E. Osawa, K. Kanematsu in *Molecular Structure and Energetics, Vol. 3, Chapt. 7* (Eds.: J. F. Liebman, A. Greenberg), VCH, Weinheim, **1986**, pp. 329–369.

[23] This effect formally corresponds to the anomeric effect in carbohydrate chemistry, but the latter uses n/σ* orbital interaction instead of electrostatic interaction [25].

[24] a) A. J. Kirby, *The Anomeric Effect and Related Stereoelectronic Effects at Oxygen*, Springer, Berlin, **1983**, p. 149; b) P. Delongchamps, *Stereoelectronic Effects in Organic Chemistry*, Pergamon Press, Oxford, **1983**, p. 375; c) E. Juaristi, G. Cuevas, *Tetrahedron* **1992**, *48*, 5019–5087; d) P. P. Graczyk, M. Mikolajczyk, *Top. Stereochem.* **1994**, *21*, 159–349.

[25] For related effects in Lewis acid complexes, see: J. Goodman, *Tetrahedron Lett.* **1992**, *33*, 7219–7222.

[26] S. Glasstone, K. J. Laidler, H. Eyring, *The Theory of Rate Processes*, MacGraw Hill, New York, **1941**, p. 611.

[27] M. J. Frisch, G. W. Trucks, M. Head-Gordon, P. M. W. Gill, M. B. Wong, J. B. Foresman, B. G. Johnson, H. B. Schlegel, M. A. Robb, E. S. Replogle, R. Gomprets, J. S. Andres, K. Raghavachari, J. S. Binkley, C. Gonzalez, R. L. Martin, D. J. Defrees, J. Baker, J. J. Stewart, J. A. Pople, Gaussian-92; Gaussian Inc. Pittsburgh, PA, 1992.

[28] R. Poirier, R. Kari, I. G. Csizmadia, *Handbook of Gaussian Basis Sets*, Elsevier, Amsterdam, **1985**, p. 674.